RAPID COMMUNICATION

Reaction mechanisms for dithiothreitol as a measure of particulate matter induced oxidative potential activity by density functional theory

Yiling Bei* and Qingyang Liu**,†

*School of Chemistry and Chemical Engineering, Shandong University, Jinan 250100, China
**Beijing Center for Physical and Chemical Analysis, Beijing 100089, China

Abstract−The measurement of particulate matter induced oxidative potential activity by dithiothreitol (DTT) as an alternative quantitative method has been of recent interest. The mechanism of this process is not well understood. Proposed mechanisms often involve formation of the hydrogen peroxide as the final step. Evidence suggests that this may not be the dominant route. We applied computational methods to determine a possible alternative mechanism in the presence of •OH radical production. An energetically favored mechanism was found for DTT-chemical reactivity reaction which is consistent with previously reported experimental results.

Keywords: Particulate Matter, Dithiothreitol, Oxidative Potential Activity, Density Functional Theory
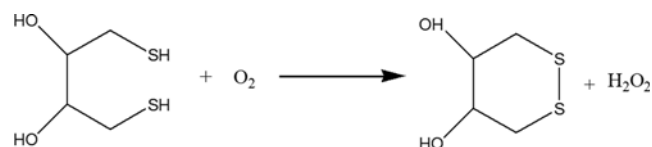
INTRODUCTION

The positive associations between particulate matter (PM) and adverse health outcomes are supported by numerous studies [1-3]. The mechanisms of PM-related health effects have not been explained clearly, but an outstanding hypothesis is that many of the adverse health effects may derive from oxidative stress [4-7]. Thus, the measurement of PM induced oxidative stress is a key factor in evaluating PM-related health effects at the beginning step. One measurement approach is the use of the dithiothreitol (DTT)-based chemical reactivity as a quantitative method for the assessment of the capacity of a PM sample to catalyze ROS generation [1,8-12]. Cho et al. [4] demonstrated that the DTT assay can provide a good measure of the redox activity by determining reactive oxygen species (ROS) formation (Scheme 1).

In this assay, reduced DTT is oxidized to its disulfide in the presence of ROS generated by PM. After the reaction, the remaining reduced DTT is reacted with 5, 5′-dithiobis(2-nitrobenzoicacid) to produce a chromophore that absorbs light at 412 nm. The rate of DTT consumption is proportional to the oxidative activity of the PM sample. Previous studies have demonstrated that three reactive oxygen species in PM samples, such as superoxide, hydrogen peroxide and hydroxyl radical, have been measured using DTT assay [8,9]. Cho et al. [4] observed that carbonaceous species, such as organic carbon, water soluble carbon and quinones in PM samples was highly correlated with DTT loss, indicating these chemical species were redox active. Charrier and Anastasio [8] have estimated that for typical PM samples approximately 80% of DTT loss is from transition metals (especially copper and manganese), while quinines account for approximately 20%. In some cases, some metals were found to not be sensitive to DTT loss [4]. The addition of a low concentration (50 nM) of iron or cooper into the PM extracts did not increase the rate of DTT oxidation [4]. In addition, Lin and Yu [9] reported that Cu (II) and Zn (II) concentration was strongly correlated with DTT loss, but not from Fe. They proposed that these metals could catalyze ambient PM to generate ROS species production, such as hydrogen peroxide and hydroxyl radical. While most of the current literature indicates that DTT assay did not respond strongly to some species of PM, especially Fe [8,11]. However, results from *in vivo* assays reported the increase of ROS production by PM has also been linked to the content of Fe. These results suggest there is a difference between the DTT assay and other measurements of the oxidative potential of PM, although the assays should be measuring similar properties of PM [8]. These results raise an interesting question for the possibility that an alternative reaction mechanism may be dominant.

Our objective was to use computational methods to afford reasonable alternative mechanisms for the dithiothreitol (DTT)-based chemical reactivity. These mechanisms start with molecular reactant shown in Eq. (1). Although the computational method used does not provide accurate quantitative values, it does provide relative values that can be compared with each other and used to determine if the proposed mechanism is energetically favored. It is hoped that the results obtained in this study will help to increase understanding of the mechanism of the dithiothreitol (DTT)-based chemical reactivity. A well understood mechanism may help to improve the technique by suggesting routes to increase efficiency, avoid or reduce interferences, and expand the method.

Scheme 1. Proposed reaction mechanism by Cho et al.

THEORETICAL METHODS

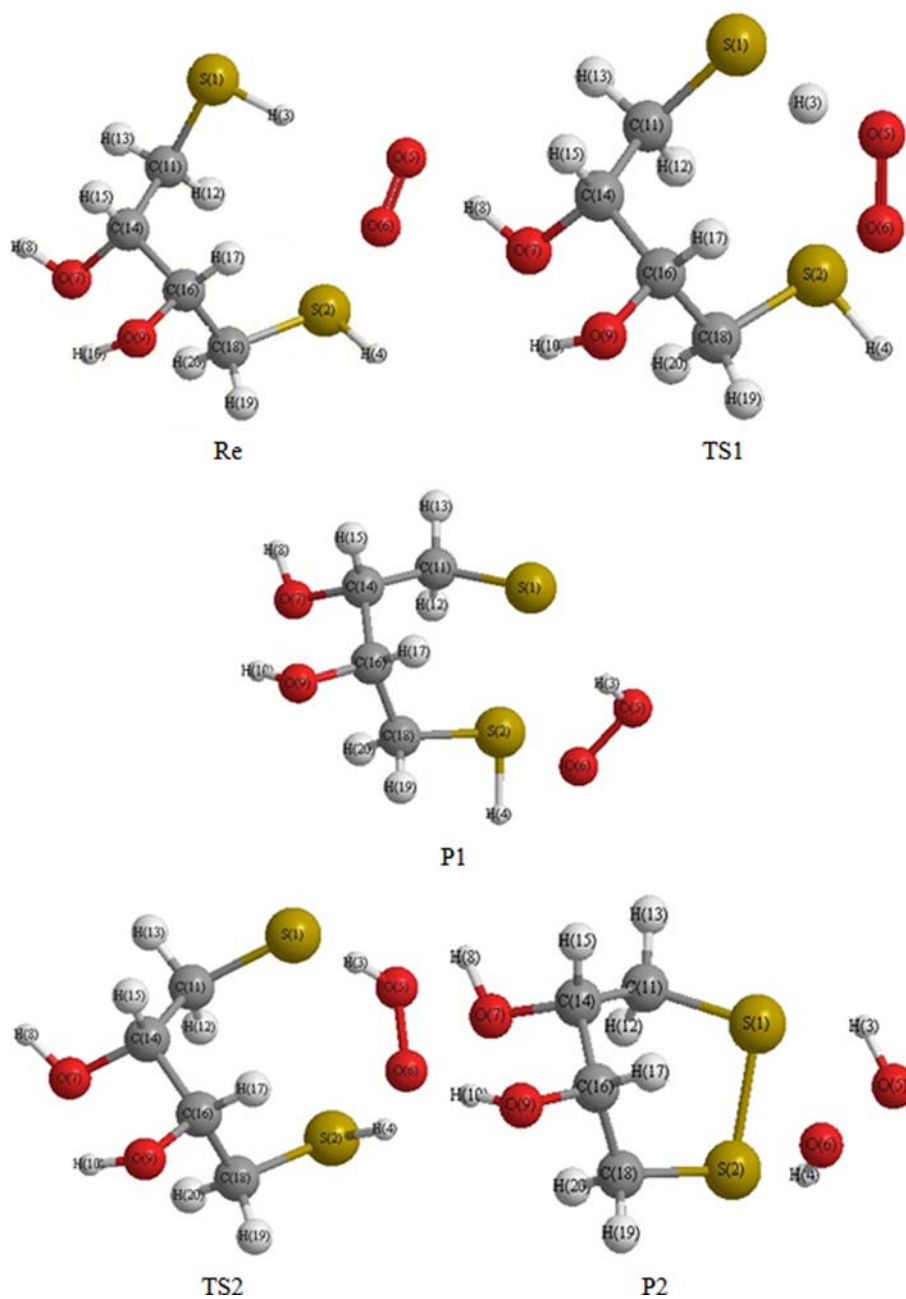The ground-state geometries of all the molecules studied opti-

Fig. 1. The geometries of reactants, transition states and final products calculated at the B3LYP/6-311G (d,p) level.
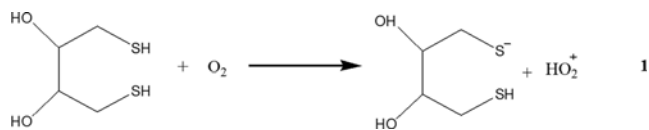
mized at the B3LYP/6-311G(d, p) level of theory are shown in Fig. 1. The geometries of various stationary points and harmonic vibrational frequencies were calculated at the same level. Only one imaginary frequency for each transition state could be found. The reaction pathways were investigated and confirmed by intrinsic reaction coordinate (IRC) calculation at the B3LYP/6-311G(d, p) level. The changes of thermodynamic functions including entropy, enthalpy, free energies for reactants, transition states and products, and the equilibrium constants of the reaction in Eyring transition state theory were calculated at the B3LYP/6-311G(d, p) level. Reaction rate constants (k(T)), changes ($\Delta S\#$, $\Delta H\#$ and ΔG) in thermodynamic functions and equilibrium constants of the reactions were calculated using the B3LYP/6-311G(d,p)-optimized geometries and the harmonic vibrational frequencies. The rate constant is given by k(T)=(k_bT/h)

exp($\Delta S\#/R-\Delta H\#/RT$), where k_b and h are the Boltzmann and Planck constants, respectively, $\Delta H\#$ is the activation enthalpy of the transition states, and $\Delta S\#$ is the activation entropy of the transition states. The reaction equilibrium constant is calculated by K=exp($-\Delta G\times$ 1000/RT), where ΔG is the Gibbs free energy of the reaction. In the preset study all kinetic and thermodynamic calculations were performed using Gaussian 03 series [13].

RESULTS AND DISCUSSION

1. Dehydrogenation Reaction

An alternative mechanism for the oxidation reaction starting with dehydrogenation reaction of DTT is shown in Scheme 2. The overall reaction surface for this process is endothermic energy favor-

Scheme 2. Proposed mechanisms for the oxidation reaction starting with dehydrogenation reaction of DTT.
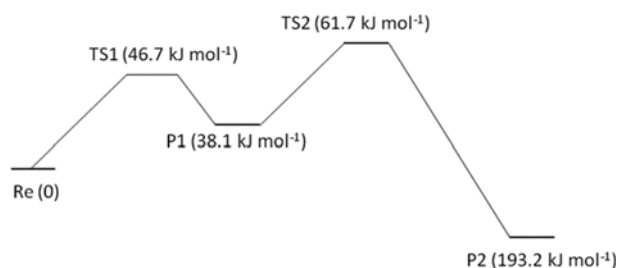

Fig. 2. The energy profiles for DTT-based chemical reactivity as a quantitative method for the assessment of the capacity of a PM sample to catalyze ROS generation. The energy values are expressed in kJ mol^{-1} and are relative to reactants.

able with a net change in energy of 38.1 kJ mol^{-1} (Fig. 2).

The first-order saddle points TS1, the transition state from Re to P1, was verified by IRC calculation. In the reaction of Re to P1, the hydrogen atom detached from the -SH group at the beginning of the reaction, resulting in the increased distances between S(1) and H(3) (from 1.349 to 1.643 Å), forming TS1. IRC calculation showed that in the reaction of Re to TS1, the hydrogen atom moved to oxygen atom, breaking the S-H bond. Simultaneously, the distance S(1)-S(2) was shortened and became a TS1 with a negative charge in which the distance S(2)-H(4) increased from 1.345 to 1.348 Å (Table 1). Compared with Re, the distances H(4)-O(6) and H(3)-O(5) decreased from 2.520 to 2.514 Å and from 2.278 to 1.177 Å, respectively. The activation barrier from Re to P1 was 46.7 kJ mol^{-1}. After getting over the TS1, the distances S(1)-S(2) and H(4)-O(6) decreased from 3.475 to 2.579 Å and from 2.514 to 2.024 Å, respectively. Meanwhile, the distance O(5)-O(6) and S(2)-H(4) increased from 1.289 to 1.396 Å and from 1.348 to 1.385 Å, respectively. At the end of reaction, the molecular HO$_2^+$ and C$_4$H$_9$O$_2$S$_2^-$ were produced. Through the calculation for above reaction pathway, the obtained results indicated that the more positive H was, and negative the atom S became, making a weaker S(1)-H(3) bond reach the transition state more easily (Table 2). Generally, kinetic and thermodynamic analyses may illustrate the feasibility and likelihood of such reactions. The kinetic and thermodynamic calculations for the optimized parameters, zero-point-corrected energies, scaled vibrational frequencies, and Hessian matrix in canonical variational-state the-

Table 2. Absolute energies, zero-point energies and relative energies of reactants, intermediates, transition states and products calculated at the B3LYP/6-311G(d,p) level

Species	E$_{ZPVE}$/ (kJ mol^{-1})	B3LYP/6-311G (d, p)		
		E/a.u.	E$_T$/a.u.	E$_R$/(kJ mol^{-1})
Re	383.8199	−1255.7104	−1255.5642	0.0
TS1	379.4996	−1255.6909	−1255.5464	46.7339
P1	397.1789	−1255.7010	−1255.5497	38.0698
TS2	391.6632	−1255.6899	−1255.5407	61.6993
P2	402.0918	−1255.7909	−1255.6378	−193.2368

Table 3. The kinetic properties and thermodynamic properties of the reaction step 1 calculated at the B3LYP/6-311G(d,p) level

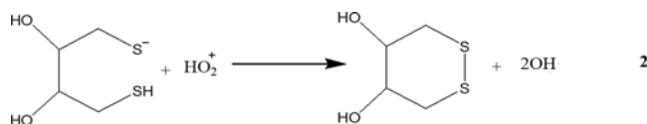| T/K	Rate constants k(T) (s^{-1})	Equilibrium constants K(T)	Changes of free energy (ΔG) (kJ mol^{-1})
400	3.59×10^4	4.64×10^{-8}	56.15
500	5.08×10^5	3.10×10^{-7}	62.30
600	2.97×10^6	1.07×10^{-6}	68.57
700	1.06×10^7	2.56×10^{-6}	74.92
800	2.74×10^7	4.89×10^{-6}	81.33
900	5.80×10^7	8.05×10^{-6}	87.77
1000	1.06×10^8	1.19×10^{-5}	94.24
1100	1.74×10^8	1.65×10^{-5}	100.74
1200	2.64×10^8	2.14×10^{-5}	107.25
1300	3.76×10^8	2.68×10^{-5}	113.78
1400	5.10×10^8	3.24×10^{-5}	120.33
1500	6.65×10^8	3.81×10^{-5}	126.89

ory (CVT) with small tuning approximation (SCT) over the temperature range of 400-1,500 K were carried out at the B3LYP/6-311G(d,p) level (Table 3). As shown in Table 3, the calculations showed that the kinetic constants increased slightly with the temperature increasing. In addition, the equilibrium constant of the reaction was very small, indicating thermodynamics feasibility of reverse reaction existed. This discrepancy can be resolved if the external energy supply is greater than the reaction barrier in step 1, thus making C$_4$H$_9$O$_2$S$_2^-$ the kinetically favored product.

2. Formation of Disulfide

The formation of disulfide starting initially with HO$_2^+$, reacts directly with C$_4$H$_9$O$_2$S$_2^-$ to yield C$_4$H$_8$O$_2$S$_2$ (Scheme 3). The overall reaction surface described by Scheme 3 is energetically favorable by 196.3 kJ mol^{-1}.

Table 1. The structural parameters calculated at the B3LYP/6-311 G(d,p) leve [bond length: Å; bond angle: (°); dihedral: (°)]

Species	S(1)-H(3)	S(2)-H(4)	S(1)-S(2)	H(3)O(5)	H(4)O(6)	O(5)O(6)	S(1)H(3)O(5)	S(2)H(4)O(6)	S(1)H(3)O(5)O(6)	S(2)H(4)O(6)O(5)
Re	1.349	1.345	4.333	2.278	2.520	1.225	171.4	83.4	−178.2	−65.8
TS1	1.643	1.348	3.475	1.177	2.514	1.289	154.0	66.3	−107.8	−46.6
P1	2.631	1.385	2.579	0.971	2.024	1.396	88.5	63.8	−86.5	−34.8
TS2	2.439	1.374	3.270	0.976	1.763	1.345	75.1	146.4	−124.3	−42.6
P2	3.035	2.460	2.138	0.967	0.974	1.452	106.0	150.2	−79.1	−76.1

Scheme 3. Proposed mechanism for disulfide formation.

Table 4. The kinetic properties and thermodynamic properties of the reaction step 2 calculated at the B3LYP/6-311G(d,p) level

T/K	Rate constants $k(T)$ (s^{-1})	Equilibrium constants $K(T)$	Changes of free energy (ΔG) (kJ mol^{-1})
400	4.83×10^9	7.66×10^{31}	−244.15
500	2.33×10^{10}	8.73×10^{25}	−248.30
600	6.77×10^{10}	9.58×10^{21}	−252.48
700	1.46×10^{11}	1.42×10^{19}	−256.66
800	2.60×10^{11}	1.07×10^{17}	−260.83
900	4.10×10^{11}	2.40×10^{15}	−264.98
1000	5.91×10^{11}	1.14×10^{14}	−269.10
1100	7.98×10^{11}	9.41×10^{12}	−273.20
1200	1.03×10^{12}	1.17×10^{12}	−277.28
1300	1.27×10^{12}	2.02×10^{11}	−281.33
1400	1.53×10^{12}	4.44×10^{10}	−285.37
1500	1.79×10^{12}	1.20×10^{10}	−289.38

When HO_2^+ attacked the $C_4H_9O_2S_2^-$ from the front of S(2), the bond S(2)-H(4) broke first, with positive charge H(4) left S(2) and moved forwards the electron deficient HO_2^+, forming disulfide and •OH radicals. This route was exothermic and the potential barriers were very low. The kinetic results for Scheme 3 indicated that the reaction proceeded at a high rate. In addition, the equilibrium constants reported herein suggest that formation of disulfide is thermodynamically more favorable (Table 4).

Interestingly, our results showed that the products for DTT reaction were a little different and to be significant. The formation of hydrogen peroxide in the process of DTT reaction was reported by previous studies (Eq. (1)). Thus, we developed the formation of hydrogen peroxide in the presence of disulfide at the beginning step and found •OH radicals instead of hydrogen peroxide, were energetically favored. According to these mechanisms, DTT could not react readily with the hydroxyl radical and ultimately formed the disulfide species, which led to the increased DTT activity observed.

Recently, many studies have revealed associations between hydroxyl radical production with Fe contents of PM [14,15]. Production of PM associated hydroxyl radicals may also be related to the generation of surface-associated environmentally persistent free radicals through Fenton reaction [14]. It is noteworthy that these associations persisted even after adjustment for individual environmental factors. Kelley et al. [16] proposed that •OH radicals formed on the surface of the particles redox cycle to produce first the superoxide and then, via Fenton reactions, and then finally the hydroxyl radicals.

Evidence in support for our findings that DTT could not react readily with the hydroxyl radical is provided by studies conducted by Lin and Yu [9]. In their studies, the increase of Fe concentration could not influence the consumption rate of DTT concentration. Studies presented here highlighted that some species such as Fe may

indeed redox cycle to produce ROS that can be maintained in biological environments, but that the selection of assays for the measurement of ROS is critical to the interpretation of data obtained in these types of experiments.

CONCLUSIONS

Alternative mechanisms have been suggested for the oxidation reaction of DTT as a quantitative method for the assessment of the capacity of a PM sample to catalyze ROS generation. These mechanisms rely on disulfide and •OH radicals as oxidation products, rather than the previously suggested hydrogen peroxide. Although there are limitations to the B3LYP method for solvent calculations, the limitations do not influence the calculation results. The qualitative aspects of the energy surfaces presented herein suggest the proposed mechanisms are reasonable. Although only oxygen has been studied in this work, similar reaction mechanisms might be expected. In our work we have not been able to prove or disprove these mechanisms experimentally. We therefore offer these proposed mechanisms for others to consider and investigate experimentally.

ACKNOWLEDGEMENTS

REFERENCES

1. M. Arhami, M. C. Minguillon, A. Polidori, J. J. Schauer, R. J. Delfino and C. Sioutas, *Indoor Air*, **20**, 17 (2010).
2. J. Baumgartner, J. J. Schauer, M. Ezzati, L. Lu, C. Cheng and J. A. Patz, *Environ. Health Persp.*, **119**, 1390 (2011).
3. J. Lewtas, *Mutat. Res.*, **636**, 95 (2007).
4. A. K. Cho, C. Sioutas, A. H. Miguel, Y. Kumagai, D. A. Schmitz, M. Singh, A. Eiguren-Fernandez and J. R. Froines, *Environ. Res.*, **99**, 40 (2005).
5. L. Ntziachristos, J. R. Froines, A. K. Cho and C. Sioutas, *Part. Fibre Toxicol.*, **4**, 5 (2007).
6. J. D. Sacks, L. W. Stanek, T. J. Luben, D. O. Johns, B. J. Buckley, J. S. Brown and M. Ross, *Environ. Health Persp.*, **119**, 446 (2011).
7. Y. J. Park, L. J. Lim and H. Song, *Environ. Eng. Res.*, **18**, 139 (2013).
8. J. G. Charrier and C. Anastasio, *Atmos. Chem. Phys.*, **12**, 9321 (2012).
9. P. Lin and J. Z. Yu, *Environ. Sci. Technol.*, **45**, 10362 (2011).
10. R. D. McWhinney, K. Badali, J. Liggio, S. M. Li and J. P. Abbatt, *Environ. Sci. Technol.*, **47**, 3362 (2013).
11. V. Verma, R. Rico-Martinez, N. Kotra, L. King, J. Liu, T. W. Snell and R. J. Weber, *Environ. Sci. Technol.*, **46**, 11384 (2012).
12. W. Kam, Z. Ning, M. M. Shafer, J. J. Schauer and C. Sioutas, *Environ. Sci. Technol.*, **45**, 6769 (2011).
13. M. J. Frisch, G. W. Trucks, H. B. Schlegel, G. E. Scuseria, M. A. Robb, J. R. Cheeseman, J. A. Montgomery, T. Vreven, K. N. Kudin, J. C. Burant, J. M. Millam, S. S. Iyengar, J. Tomasi, B. Mennucci, M. Cossi, G. Scalmani, N. Rega, G. A. Petersson, H. Nakatsuji, M. Hada, M. Ehara, K. Toyota, R. Fukuda, J. Hasegawa, M. Ishida, T. Nakajima, Y. Honda, O. Kita, H. Nakai, M. Klene, X. Li, J. E. Knox, H. P.

Hratchian, J. B. Cross, V. Bakken, C. Adamo, J. Jaramillo, R. Gomperts, R. E. Stratmann, O. Yazyev, A. J. Austin, R. Cammi, C. Pomelli, J. W. Ochterski, P. Y. Ayala, K. Morokuma, G. A. Voth, P. Salvador, J. J. Dannenberg, V. G. Zakrzewski, S. Dapprich, A. D. Strain, M. C. Farkas, O. Malick, D. K. Rabuck, A. D. Raghavachari, K. Foresman, J. B. Ortiz, Q. Cui, A. G. Baboul, S. Cliolord, J. Cioslowski, B. B. Stefanov, G. Liu, A. Liashenko, P. Piskorz, I. Komaromi, R. L. Martin, D. J. Fox, T. Keith, M. A. Al-Laham, C. Y. Peng, A. Nanayakkara, M. Challacombe, P. M. W. Gill, B. Johnson, W. Chen, M. W. Wong, C. Gonzalez and J. A. Pople, Gaussian Inc., Pittsburgh, PA (2003).

14. T. L. Stoiber, M. M. Shafer and D. E. Armstrong, *Environ. Toxicol.*, **28**, 516 (2013).

15. Y. Li, T. Zhu, J. C. Zhao and B. Y. Xu, *Environ. Sci. Technol.*, **46**, 10302 (2012).

16. M. A. Kelly, V. Y. Hebert, T. M. Thibeaux, M. A. Orchard, F. Hasan, S. A. Cormier, P. T. Thevenot, S. M. Lomnicki, K. J. Varner, B. Dellinger, B. M. Latimer and T. R. Dugas. *Chem. Res. Toxicol.*, **26**, 1862 (2013).